

Missing Velocity in Dynamic Obstacle Avoidance based on Deep Reinforcement Learning

Fabian Hart^{*}, Martin Waltz^{*}, and Ostap Okhrin^{*}

^{}Institute of Transportation Economics, Technische Universität Dresden, Germany*

December 24, 2021

Abstract

We introduce a novel approach to dynamic obstacle avoidance based on Deep Reinforcement Learning by defining a traffic type independent environment with variable complexity. Filling a gap in the current literature, we thoroughly investigate the effect of missing velocity information on an agent’s performance in obstacle avoidance tasks. This is a crucial issue in practice since several sensors yield only positional information of objects or vehicles. We evaluate frequently-applied approaches in scenarios of partial observability, namely the incorporation of recurrency in the deep neural networks and simple frame-stacking. For our analysis, we rely on state-of-the-art model-free deep RL algorithms. The lack of velocity information is found to significantly impact the performance of an agent. Both approaches - recurrency and frame-stacking - cannot consistently replace missing velocity information in the observation space. However, in simplified scenarios, they can significantly boost performance and stabilize the overall training procedure.

Keywords: Dynamic Obstacle Avoidance, Deep Reinforcement Learning, POMDP, LSTM

1 Introduction

The problem of deriving a collision-free path for an agent moving among dynamic obstacles is a widely studied area and has applications in many fields of automated transportation systems, such as self-driving cars (Urmson et al., 2008), unmanned aerial vehicles (Goerzen et al., 2010), and service robots (Triebel et al., 2016). However, Canny and Reif (1987) showed that in a simple obstacle avoidance (OA) case, where a 2D holonomic robot faces dynamic polygon obstacles with constant velocities, the problem is NP-Hard. Velocity Obstacles (Fiorini and Shiller, 1998) is one of several algorithmic solutions that have been developed for the problem of dynamic OA and has been widely applied on vehicles for collision prevention, e.g., wheeled robots (Wilkie et al., 2009), unmanned aerial vehicles (Jenie et al., 2016), and unmanned surface vehicles (Kuwata et al., 2014).

At present, the advances in machine learning methods, particularly in Reinforcement Learning (RL, Sutton and Barto (2018)), provide a new possibility for navigation in dynamic environments. Especially Deep RL, which uses deep neural networks (Goodfellow et al., 2016) as function approximators, has already shown remarkable achievements, e.g., by learning to play Atari video games from pixels (Mnih et al., 2015) or by mastering the game of Go (Silver et al., 2017). These methods have also been successfully applied to the domain of obstacle avoidance: Duguleana and Mogan (2016) and Cimurs et al. (2020) use RL to compute collision-free trajectories for mobile robots in real-life environments; Wang et al. (2019) and Roghair et al. (2021) train agents to allow unmanned aerial vehicles to navigate in complex environments; Chen et al. (2019) and Xu et al. (2020) propose collision avoidance algorithms for underactuated unmanned surface vehicles using RL. Another strand of literature uses vision- or rangefinder-based information from the environment and are primarily based on convolutional neural networks to extract features about surrounding obstacles, see (Xie et al., 2017), (Cimurs et al., 2020), or (Wang et al., 2018). Furthermore, various studies (Bhopale et al., 2019; Xu et al., 2020; Yan et al., 2021) focus on RL-based OA algorithms that directly use hand-shaped features about surrounding obstacles, for example, positions or headings. Common practice is also the inclusion of velocity information about obstacles into these features, although in real applications only relative distances to obstacles can be extracted from many common sensors, e.g., camera image data. However, there is to the best of our knowledge no comprehensive comparison of how severe this velocity information loss affects the performance of the used algorithms. To stress: all aforementioned studies either do use or do not use velocity information explicitly or implicitly.

This motivated us to thoroughly compare both approaches and analyze the resulting performances of collision prevention in a generic OA environment. Furthermore, common strategies to combat velocity information deficiencies and to improve the trajectory anticipation capabilities of the agent include: 1) the use of a time-series of past environmental information; and 2) the incorporation of recurrency into the neural network structure (Althé and de La Fortelle, 2017). Therefore, we additionally analyzed whether recurrent layers can boost the overall performance if velocity information about obstacles is missing. Summarizing, the main contributions of our work are as follows:

- Introduction of a novel approach to dynamic OA based on Deep RL including the definition of a generic environment with variable complexities.

- Analysis of a sensory-motivated reduced observation space in which information about velocities is not available.
- A comprehensive comparison of state-of-the-art model-free RL algorithms for continuous action spaces with and without recurrency in the deep neural network structure.

Based on the previous research, we formulate and test the following hypotheses:

Hypothesis 1: One can use recurrent layers in the function approximation to reconstruct missing velocity information solely from positional information in an obstacle avoidance task.

Hypothesis 2: Alternatively, one could simply use frame-stacking to reconstruct missing velocity information.

This work is structured as follows: In Section 2, we give a detailed overview of the RL basics and we provide information about the used RL algorithms. In Section 3, we define the OA environment variants to test our hypotheses, followed by the results of the RL training in Section 4. The results are discussed in Section 5. Section 6 concludes.

2 Reinforcement Learning Methodology

2.1 Basics

RL aims at solving sequential decision tasks in which an agent interacts with an environment under the objective to maximize the received reward (Sutton and Barto, 2018). Formally, we consider Markov Decision Processes (MDP) consisting of a state space \mathcal{S} , an action space \mathcal{A} , an initial state distribution $T_0 : \mathcal{S} \rightarrow [0, 1]$, a state transition probability distribution $\mathcal{P} : \mathcal{S} \times \mathcal{A} \times \mathcal{S} \rightarrow [0, 1]$, a reward function $\mathcal{R} : \mathcal{S} \times \mathcal{A} \rightarrow \mathbb{R}$, and a discount factor $\gamma \in [0, 1]$. At each time step t , the agent receives a state information $S_t \in \mathcal{S}$, selects an action $A_t \in \mathcal{A}$, gets a reward R_{t+1} , and transitions based on the environmental dynamics \mathcal{P} to the next state $S_{t+1} \in \mathcal{S}$. Furthermore, we consider Partially Observable Markov Decision Processes (POMDP, Kaelbling et al. (1998)), which generalize the MDP by introducing two additional components: the observation space \mathcal{O} and the observation function $\mathcal{Z} : \mathcal{S} \times \mathcal{A} \times \mathcal{O} \rightarrow [0, 1]$. In a POMDP, the agent does not receive the new state S_{t+1} directly, but instead an observation $O_{t+1} \in \mathcal{O}$, which is generated with probability $P(O_{t+1}|S_{t+1}, A_t)$ by the observation function \mathcal{Z} . Consequently, a POMDP is a Hidden Markov Model with actions and the observations are used for learning. In the following, we use capital notation, e.g., S_t , to indicate random variables and small notation, e.g., s_t or s , to describe realizations.

Objective of the agent in the MDP scenario is to learn a policy $\pi : \mathcal{S} \times \mathcal{A} \rightarrow [0, 1]$, a mapping from states to probability distributions over actions, that maximizes the expected return, which is the expected discounted cumulative reward, from the start state: $E_\pi [\sum_{k=0}^{\infty} \gamma^k R_{k+1} | S_0]$. Common practice is the definition of action value functions $Q^\pi(s, a)$, which are the expected return when starting in state s , taking action a , and following policy π afterward: $Q^\pi(s, a) = E_\pi [\sum_{k=0}^{\infty} \gamma^k R_{t+k+1} | S_t = s, A_t = a]$. Crucially, in an MDP there is always a deterministic optimal policy $\pi^*(s) = \arg \max_{a \in \mathcal{A}} Q^*(s, a)$, that is connected with

an optimal action-value function $Q^*(s, a) = \max_{\pi} Q^{\pi}(s, a)$. To learn $Q^*(s, a)$, a recursive relationship termed Bellman optimality equation (Bellman, 1954) is frequently used:

$$Q^*(s, a) = \mathcal{R}(s, a) + \gamma \sum_{s' \in \mathcal{S}} \mathcal{P}_{sa}^{s'} \max_{a' \in \mathcal{A}} Q^*(s', a'). \quad (1)$$

The popular Q-Learning algorithm (Watkins and Dayan, 1992) translates (1) into a sample-based update procedure. The Q-values are approximated by tabular representations, which store a particular value for each (s, a) -pair. However, this approach is not feasible for continuous state spaces, which is why more complex representations like deep neural networks are used to approximate the Q-values. This serves as a basis for the Deep Q-Network (DQN, Mnih et al. (2015)), which is a fundamental approach to combine Q-Learning with function approximation. Having a function $Q^{\omega}(s, a)$ with parameter vector ω , the training is realized by gradient descent:

$$\omega \leftarrow \omega + \alpha \{y - Q^{\omega}(s, a)\} \nabla_{\omega} Q^{\omega}(s, a), \quad (2)$$

with reward r , target $y = r + \gamma \max_{a' \in \mathcal{A}} Q^{\omega'}(s', a')$, and learning rate α . $Q^{\omega'}(s, a)$ is referred to as the target network and can greatly stabilize the training process. It is a time-delayed copy of the original network with parameter ω . Furthermore, DQN uses experience replay, in which past transitions are sampled randomly (or with more sophisticated strategies like Schaul et al. (2016)) to perform gradient descent steps. However, DQN is restricted to discrete action spaces \mathcal{A} since it involves calculating the maximum over all possible actions. Our application case involves continuous actions spaces, which is the reason we use the state-of-the-art TD3 algorithm (Fujimoto et al., 2018). Its functionality is detailed in the following.

2.2 Twin Delayed Deep Deterministic Policy Gradient (TD3)

The TD3 is an extension of the Deep Deterministic Policy Gradient (DDPG) algorithm of Lillicrap et al. (2015). The DDPG is an off-policy, actor-critic algorithm that uses neural networks as function approximators. Importantly, it is based on a *deterministic* policy $\mu^{\theta} : \mathcal{S} \rightarrow \mathcal{A}$ with parameter vector θ . In this setup μ^{θ} takes the role of the actor and approximates the maximum operation in the target computation. The second component of the framework is the critic function $Q^{\omega}(s, a)$, which approximates the action-values as in the DQN and is updated by gradient descent. In this context, the critic will be used to evaluate the actions made by the actor. More precisely, we consider the performance objective based on the deterministic policy: $J(\mu^{\theta}) = E_{\mu^{\theta}} [\sum_{k=0}^{\infty} \gamma^k R_{k+1} | S_0]$. Silver et al. (2014) proved the *Deterministic Policy Gradient Theorem*, which yields the gradient of the performance measure with respect to θ :

$$\nabla_{\theta} J(\mu^{\theta}) \approx E_{s \sim \rho^{\mu}} \{ \nabla_{\theta} \mu^{\theta}(s) \nabla_a Q^{\omega}(s, a) |_{a=\mu^{\theta}(s)} \}, \quad (3)$$

where ρ^{μ} is the discounted state visitation distribution. This gradient can be used to train the actor via gradient ascent, so that both actor and critic are updated iteratively. Furthermore, Lillicrap et al. (2015) proposed to also use experience replay and target networks. However, a soft-update of the target networks for both actor and critic is applied, which constrains the

update targets to change slowly and yields a further stabilized training procedure. Denoting τ as the soft target update rate, θ' and ω' the parameter sets of the target actor and critic, respectively, the update is:

$$\begin{aligned}\omega' &= \tau\omega + (1 - \tau)\omega', \\ \theta' &= \tau\theta + (1 - \tau)\theta'.\end{aligned}\tag{4}$$

Exploration is performed by perturbing the action of the actor with additional random noise. However, [Fujimoto et al. \(2018\)](#) introduced three modifications of the original DDPG to receive a state-of-the-art model-free algorithm. First, the TD3 uses the minimum of two critics $Q^{\omega_1}(s, a)$ and $Q^{\omega_2}(s, a)$ to combat the overestimation issue in the critic update. Second, the variance of the critic update is reduced by introducing target policy smoothing. Consequently, while the critic target in DDPG was $y = r + \gamma Q^{\omega'}\{s', \mu^{\theta'}(s')\}$, the TD3 uses $y = r + \gamma \min_{i=1,2} Q^{\omega'_i}\{s', \mu^{\theta'}(s') + \tilde{\epsilon}\}$ with $\tilde{\epsilon} \sim \text{clip}\{\mathcal{N}(0, \tilde{\sigma}), -c, c\}$ for some $c > 0$, and normal distribution \mathcal{N} with standard deviation $\tilde{\sigma}$. Third, instead of performing policy and target updates at every step, the TD3 typically performs them only every $d = 2$ steps, which was shown to yield improved performance. The complete algorithm is detailed in [Appendix A](#).

2.3 Long-Short-Term-Memory (LSTM) based TD3

As described in [Section 2.1](#), only observations o_t rather than full states s_t are available in the POMDP case. One popular approach to handle this scenario is the construction of belief states, which are distributions over the real states the agent might be in, given the observation so far. However, this requires a model of the environment and is computationally demanding ([Heess et al., 2015](#)). An alternative approach might be to stack past observations together (see [Mnih et al. \(2015\)](#)) and use this as input for the network. This frame-stacking (FS) technique will also be investigated in [Section 4](#), where we equip the TD3 algorithm with past observations and refer to it as TD3-FS. However, it is not immediately obvious which information will be of relevance later on, and all past observations are equally weighted when simply expanding the input vector. Finally, a further approach is to incorporate recurrency into the function approximators of model-free algorithms, which was shown to be capable of strong performances ([Ni et al., 2021](#)). The recurrency enriches the agent’s decision making by extracting information of past observations, potentially yielding an improved ability to solve problems without access to the complete state vector. Concretely, [Meng et al. \(2021\)](#) proposed an extension of the TD3 called LSTM-TD3, which adds LSTM layers ([Hochreiter and Schmidhuber, 1997](#)) to actor and critic of the TD3. The resulting algorithm showed impressive results on several benchmark tasks from the continuous action domain. We adapt it as our memory-based model-free competitor to the TD3.

In the following, we use the notation o_t instead of s_t since the LSTM-TD3 was developed to tackle POMDP scenarios. However, in the dynamic OA scenario detailed in [Section 3](#), we test all approaches (TD3, TD3-FS, LSTM-TD3) with full state and reduced observation input, respectively. To describe the functionality of LSTM-TD3, we define the past history

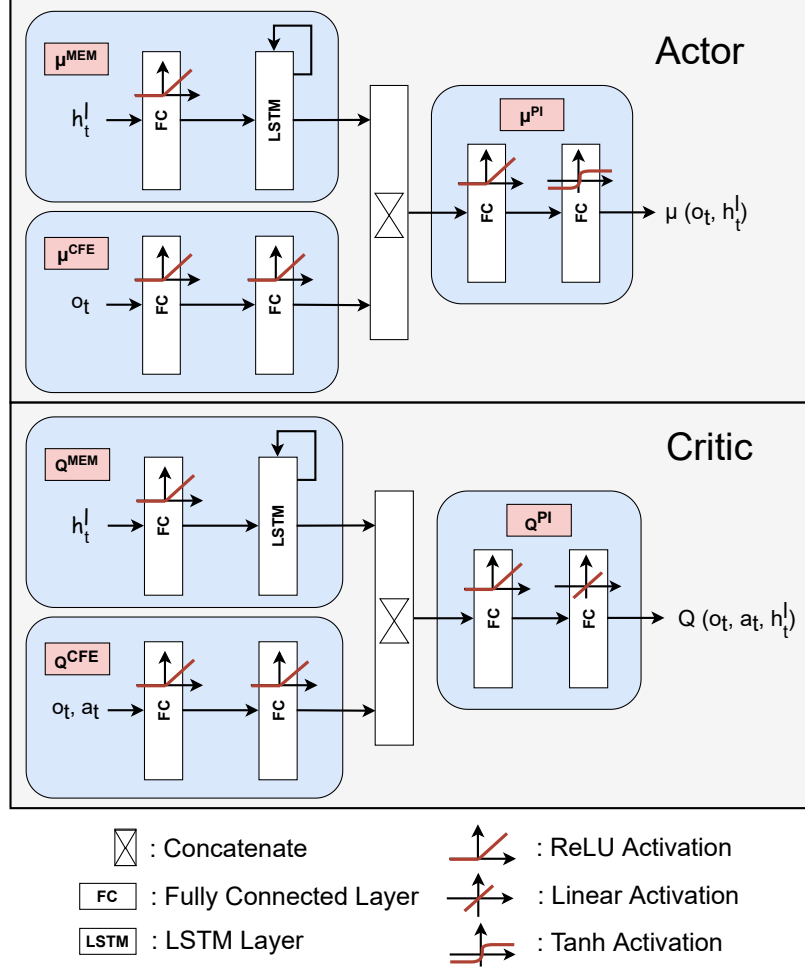


Figure 1: Illustration of the implemented LSTM-TD3 network architecture, adapted from Meng et al. (2021). MEM abbreviates memory extraction, CFE is current feature extraction, and PI refers to perception integration. Note that with *one layer*, we mean *one weight connection matrix*, as it is specified when implementing the architecture in deep learning frameworks like PyTorch (Paszke et al., 2019) or Tensorflow (Abadi et al., 2016). This illustration format is chosen since it immediately enables reproducibility.

h_t^l of length l at time step t as:

$$h_t^l = \begin{cases} o_{t-l}, \dots, o_{t-1} & \text{if } l, t \geq 1. \\ o_0 & \text{else.} \end{cases} \quad (5)$$

o_0 is a zero-valued dummy observation of the same dimension as a regular observation. Note that the definition of h_t^l slightly differs from Meng et al. (2021) since we do not include past actions in the history. Furthermore, we set $l = 2$ throughout the paper, because, from a physical perspective, velocity and acceleration of an obstacle can be estimated based on its current and two last positions. The algorithm disassembles both actor and critic into different sub-components. Precisely, there is a memory extraction (MEM) part in the

function approximators, Q^{mem} and μ^{mem} , respectively, that processes the history. In parallel, the current feature extraction (CFE) components Q^{cfe} and μ^{cfe} process the observation of the current step o_t . Finally, the output of both MEM and CFE are concatenated and fed into the perception integration (PI) components Q^{pi} and μ^{pi} . These aggregate the extracted pieces of information and yield the final result. The complete network design of our LSTM-TD3 implementation is illustrated in Figure 1 and formalized as follows:

$$Q(o_t, a_t, h_t^l) = Q^{pi} \{ Q^{me}(h_t^l) \bowtie Q^{cfe}(o_t, a_t) \}, \quad (6)$$

$$\mu(o_t, h_t^l) = \mu^{pi} \{ \mu^{me}(h_t^l) \bowtie \mu^{cfe}(o_t) \}, \quad (7)$$

where \bowtie is the concatenation operator. The remaining optimization and training process follows the one of the TD3. Algorithm 1 summarizes the procedure.

2.4 Implementation and Initial Example

All algorithms and environments shown in this paper are implemented in Python while using the deep learning framework PyTorch (Paszke et al., 2019). Optimization is performed with Adam (Kingma and Ba, 2014). The complete list of hyperparameters is given in Appendix A, while we specify the network structure of the TD3 as in the original proposal of Fujimoto et al. (2018). To initially validate the performance potential of the LSTM-TD3 over the TD3 when POMDP cases are present, we select the `InvertedDoublePendulumPyBulletEnv-v0` environment from PyBullet-Gym (Ellenberger, 2021). This is a classic continuous control problem. More precisely, we consider the MDP version with a fully observable state-space, and the POMDP version called Remove-Velocity (RV), in which velocity-related elements of the state-vector are not available. In theory, if velocities are important to master a given task, the LSTM-TD3 algorithm should have severe advantages over the TD3 due to its processing of past information. We train each algorithm for $5 \cdot 10^6$ time steps. Every 5 000 training steps, we average the return of 10 evaluation episodes, which are played with the current deterministic policy. The whole procedure is repeated for 10 different seeds and exponentially smoothed for clarity. Figure 2 shows the results. We observe that both algorithms learn relatively fast and stable in the MDP case, and reach a similar level of final performance. However, the TD3 is clearly not able to master the given task in the RV scenario since it initially learns fast, but then drops back to a low level of performance. In contrary, the LSTM-TD3 has a longer and relatively stable learning performance, reaching a final level nearly comparable to the MDP case.

3 Approach: Obstacle Avoidance

3.1 Problem Description

To test our initial hypotheses, we propose two different obstacle avoidance environments, on which we thoroughly compare different RL algorithms. We distinguish between an MDP scenario, which includes the full state information, and an RV case, in which velocity information is not available. The main objective is to analyze the performance of the algorithms when hiding velocity information in the observation of the agent. We try to formulate general

Algorithm 1: LSTM-TD3 algorithm following [Meng et al. \(2021\)](#).

Randomly initialize critics $Q^{\omega_1}, Q^{\omega_2}$ and actor μ^θ
Initialize target critics $Q^{\omega'_1}, Q^{\omega'_2}$ and target actor $\mu^{\theta'}$ with $\omega'_1 \leftarrow \omega_1, \omega'_2 \leftarrow \omega_2, \theta' \leftarrow \theta$
Initialize replay buffer \mathcal{D}
Receive initial observation o_1 from environment, initialize history $h_1^l = \mathbf{0}$
for $t = 1, T$ **do**
 Acting
 Select action with exploration noise: $a_t = \mu^\theta(o_t, h_t^l) + \epsilon, \quad \epsilon \sim \mathcal{N}(0, \sigma)$
 Execute a_t , receive reward r_{t+1} , new observation o_{t+1} , and done flag d_t
 Store transition $(o_t, a_t, r_{t+1}, o_{t+1}, d_t)$ to \mathcal{D}

 Learning
 Sample random mini-batch of transitions with their corresponding histories
 $(h_i^l, o_i, a_i, r_{i+1}, o_{i+1}, d_i)_{i=1}^N$ from \mathcal{D}
 Calculate targets:

$$\tilde{a}_{i+1} = \mu^{\theta'}(o_{i+1}, h_{i+1}^l) + \tilde{\epsilon}, \quad \tilde{\epsilon} \sim \text{clip}\{\mathcal{N}(0, \tilde{\sigma}), -c, c\},$$

$$y_i = r_{i+1} + \gamma(1 - d_i) \min_{j=1,2} Q^{\omega'_j}(o_{i+1}, \tilde{a}_{i+1}, h_{i+1}^l).$$
 Update critics: $\omega_j \leftarrow \min_{\omega_j} N^{-1} \sum_i \{y_i - Q^{\omega_j}(o_i, a_i, h_i^l)\}^2$
 if $t \bmod d$ **then**
 Update actor: $\theta \leftarrow \max_{\theta} N^{-1} \sum_i Q^{\omega_1} \{o_i, \mu^\theta(o_i, h_i^l), h_i^l\}$
 Update target networks via (4)
 end

 End of episode handling
 if d_t **then**
 Reset environment to get initial observation o_{t+1}
 Reset history $h_{t+1}^l = \mathbf{0}$
 else
 $h_{t+1}^l = (h_t^l - o_{t-l}) \cup o_t$
 end
end

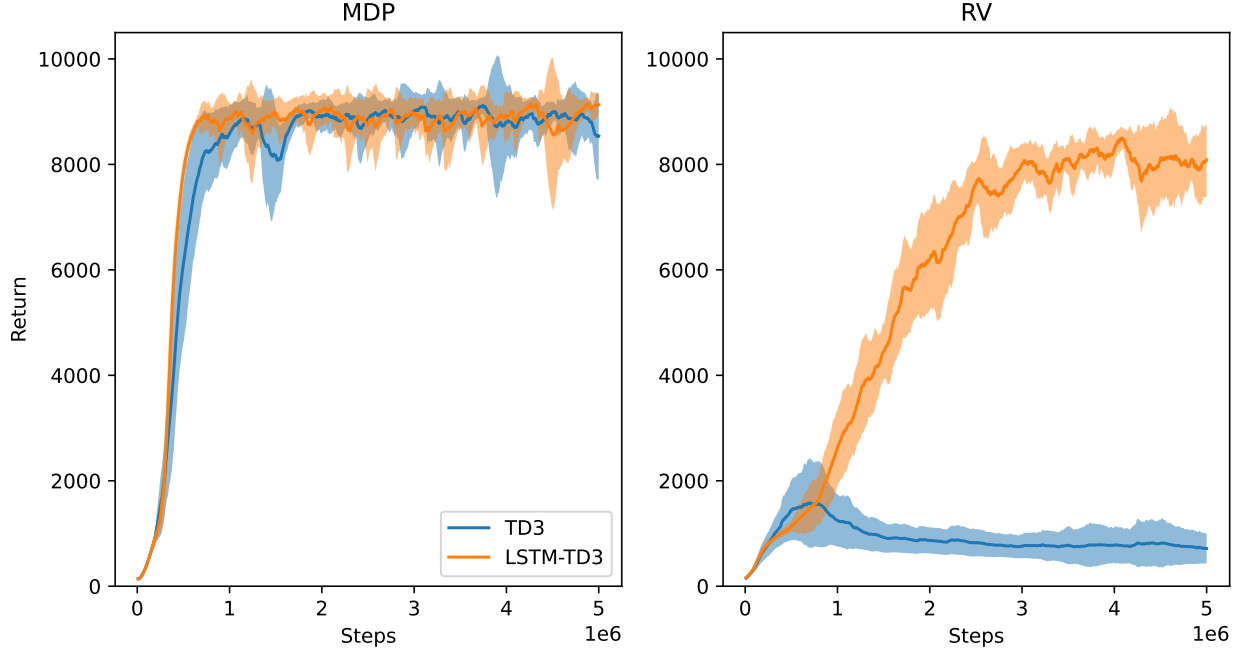


Figure 2: Performance comparison of TD3 with LSTM-TD3 for the environment `InvertedDoublePendulumPyBulletEnv-v0`. Results are averaged over 10 independent runs. The shaded area are two standard deviations over the runs.

obstacle avoidance environments that do not depend on a specific type of traffic. This leads to the following assumptions:

- The agent, as well as the obstacles, are represented as point mass models.
- The agent’s speed in the longitudinal direction is constant, while the lateral dynamics are controlled by the agent.
- The obstacle velocities are constant.
- The obstacles can be passed only in a predefined fashion, thus avoiding binary passing decisions where the agent may get stuck in between obstacles.

Under these assumptions and thinking of the obstacles as other traffic participants, we can consider our environment as a general representation of two-dimensional traffic with overtaking rules, for example, inland vessel traffic (Xu et al., 2015).

Both environments are depicted in Figure 3. The first one, Simple-OA, is a reduced scenario with two obstacles and additional constraints that allow to isolate the problem of velocity reconstruction. The second environment, Complex-OA, follows the same principles but represents a more complex and realistic obstacle avoidance environment. In the following, we describe both environmental dynamics and the corresponding simulation procedures in detail.

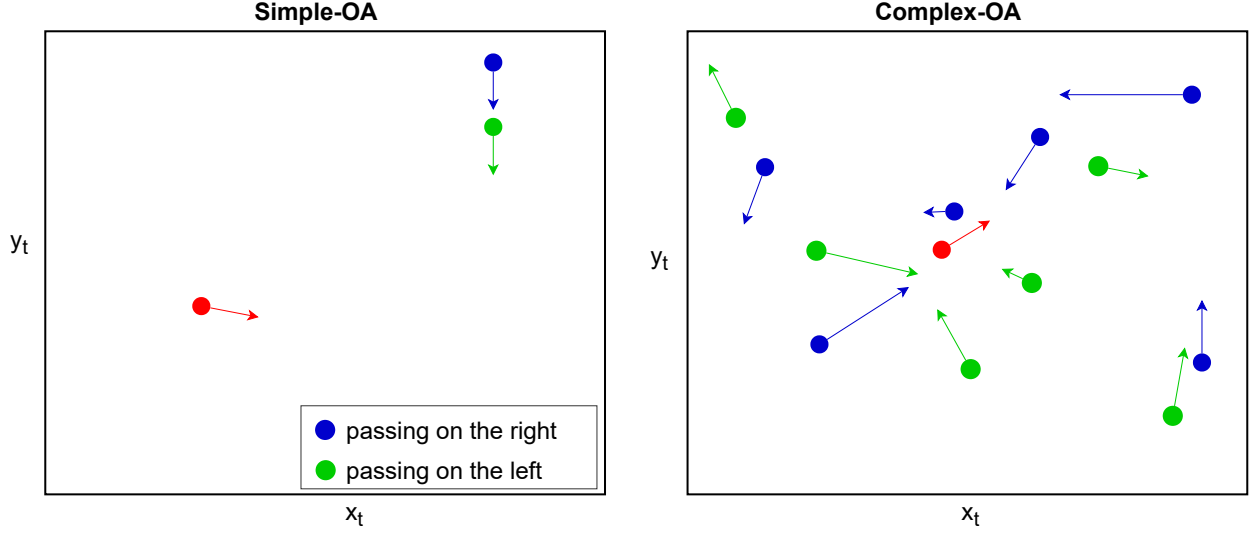


Figure 3: Environments Simple-OA and Complex-OA, where the agent is red, obstacles with passing rule 'right' are blue, and obstacles with passing rule 'left' are green. The arrows indicate direction and magnitude of velocity.

3.2 General Environment Definitions

We consider a set of obstacles $\mathcal{M} = \{1, \dots, N_{\text{obstacle}}\}$, where N_{obstacle} is the total number of obstacles in the respective environment. For each time step t , we define $x_{t,\text{agent}}$ and $x_{t,i}$ as the longitudinal position of agent and obstacle $i \in \mathcal{M}$, respectively, and $y_{t,\text{agent}}$ and $y_{t,i}$ as the corresponding lateral positions. $\dot{x}_{t,\text{agent}}$ and $\dot{x}_{t,i}$ denote the longitudinal speed, and $\dot{y}_{t,\text{agent}}$ and $\dot{y}_{t,i}$ the lateral speed for agent and obstacle $i \in \mathcal{M}$, while $\ddot{y}_{t,\text{agent}}$ is the agent's lateral acceleration. Based on those definitions, the state at time step t is defined as:

$$s_t = \begin{pmatrix} \ddot{y}_{t,\text{agent}} \\ a_{y,\text{max}} \\ \dot{y}_{t,\text{agent}} \\ v_{y,\text{max}} \\ \frac{\dot{x}_{t,\text{agent}} - \dot{x}_{t,i}}{v_{x,\text{max}}} \\ \frac{\dot{y}_{t,\text{agent}} - \dot{y}_{t,i}}{v_{y,\text{max}}} \\ \frac{x_{t,\text{agent}} - x_{t,i}}{x_{\text{scale}}} \\ \frac{y_{t,\text{agent}} - y_{t,i}}{y_{\text{scale}}} \end{pmatrix}, \quad (8)$$

where $a_{y,\text{max}}$ defines the maximum lateral acceleration for the agent, $v_{x,\text{max}}$ and $v_{y,\text{max}}$ denote maximum lateral and longitudinal speeds, and x_{scale} and y_{scale} are scaling parameters. Consequently, s_t is of dimension $2 + 4N_{\text{obstacle}}$. The values of all general parameters can be found in Table 1. We distinguish between an MDP case where the agent can observe the full state at time step t :

$$o_{t,\text{MDP}} = s_t, \quad (9)$$

Table 1: General parameters for the Environments Simple-OA and Complex-OA

Parameter	Description	Value
$\Delta a_{y,\max}$	agents maximum lateral acceleration change	0.005 m/s ²
$a_{y,\max}$	agents maximum lateral acceleration	0.01 m/s ²
$v_{x,\max}$	agents maximum longitudinal speed	5 m/s
$v_{y,\max}$	agents maximum lateral speed	5 m/s
Δt	simulation step size	5 s

and an RV case where the agent only receives positional information about the obstacles:

$$o_{t,\text{RV}} = \begin{pmatrix} \frac{\ddot{y}_{t,\text{agent}}}{a_{y,\max}} \\ \frac{\dot{y}_{t,\text{agent}}}{v_{y,\max}} \\ \frac{x_{t,\text{agent}} - x_{t,i}}{x_{\text{scale}}} \\ \frac{y_{t,\text{agent}} - y_{t,i}}{y_{\text{scale}}} \end{pmatrix}. \quad (10)$$

Based on the observation o_t , the agent computes an action $a_t \in [-1, 1]$ that is mapped to an acceleration in lateral direction:

$$\ddot{y}_{t+1,\text{agent}} = \ddot{y}_{t,\text{agent}} + \Delta a_{y,\max} a_t, \quad (11)$$

where $\Delta a_{y,\max}$ defines the maximal incremental lateral acceleration for the agent. The action can be seen as a jerk and $\Delta a_{y,\max}$ as the maximum jerk to avoid too large jumps in the acceleration of the agent. The Euler and ballistic methods are used to update the agent's lateral speed and the positions for agent and obstacles at time step $t+1$ (Treiber and Kesting, 2013). Exemplary for the agent, we have:

$$\dot{y}_{t+1,\text{agent}} = \dot{y}_{t,\text{agent}} + \ddot{y}_{t+1,\text{agent}} \Delta t, \quad (12)$$

$$x_{t+1,\text{agent}} = x_{t,\text{agent}} + \frac{\dot{x}_{t,\text{agent}} + \dot{x}_{t+1,\text{agent}}}{2} \Delta t, \quad (13)$$

$$y_{t+1,\text{agent}} = y_{t,\text{agent}} + \frac{\dot{y}_{t,\text{agent}} + \dot{y}_{t+1,\text{agent}}}{2} \Delta t, \quad (14)$$

with Δt corresponding to the simulation step size.

3.3 Environment Simple-OA

The focus of the environment Simple-OA is the isolated analysis of the anticipation of a single trajectory, leading to the specification $N_{\text{obstacle}} = 2$. The obstacles move with the same speed in the lateral direction, while the longitudinal speed is zero. Both obstacles are initialized with the same longitudinal position and the RL agent needs to pass between both obstacles, which can be interpreted as a moving finish line. Figure 4 shows a schematic representation of the environment. The optimal solution of this problem requires to simply anticipate the trajectory of the obstacle pair that moves with a constant lateral speed.

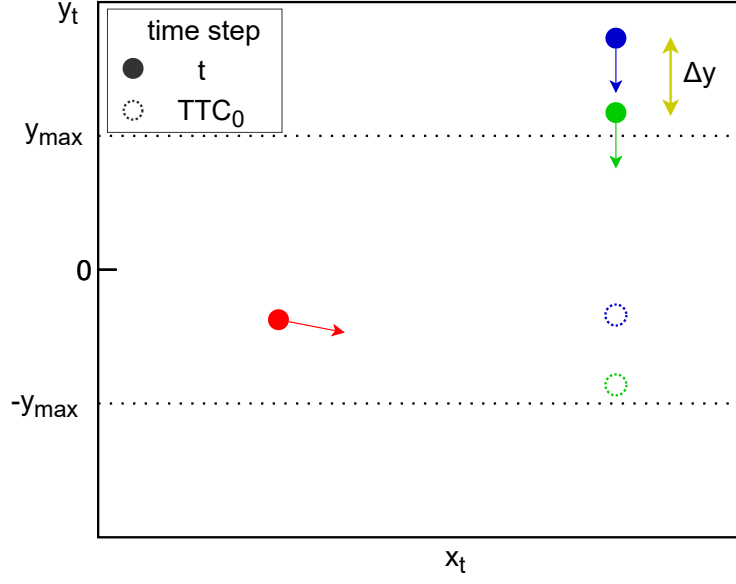


Figure 4: Environment Simple-OA with agent in red and obstacles in blue and green, respectively. The arrows indicate velocities.

We initialize the state space as follows: The agent’s dynamics are zero, except the longitudinal speed $\dot{x}_{0,agent}$, that is sampled uniformly at random from the interval $[1 \text{ m/s}, v_{x,max}]$. Further, we sample the agent’s initial time-to-collision with the obstacles in longitudinal direction, TTC_0 , uniformly at random from the interval $[280 \text{ s}, 320 \text{ s}]$. Afterward, the initial dynamics of the two obstacles are set to fulfill the following constraints:

$$\dot{y}_{t,1} \sim \mathcal{U}([-v_{y,max}, v_{y,max}]), \quad (15)$$

$$\dot{y}_{t,1} = \dot{y}_{t,2}, \quad (16)$$

$$\frac{y_{TTC_0,1} - y_{TTC_0,2}}{2} \sim \mathcal{U}([-y_{max}, y_{max}]), \quad (17)$$

$$y_{t,1} - y_{t,2} = \Delta y, \quad (18)$$

$$\dot{x}_{t,i} = 0, \quad (19)$$

where the parameters y_{max} and Δy are described in Table 2 and visualized in Figure 4.

During one episode, all velocities are kept constant, and an episode ends when:

$$x_{t,agent} > x_{t,i}. \quad (20)$$

The evaluation quantity of interest is whether the final position of the agent is between the obstacles, thus checking whether the trajectory was adequately anticipated. Consequently, we impose a non-zero reward only at the final step of an episode, leading to the following reward structure:

$$r_t = \begin{cases} 100, & \text{if } y_{t,agent} \in (y_{t,2}, y_{t,1}) \text{ and } x_{t,agent} > x_{t,i}, \\ -100, & \text{if } y_{t,agent} \notin (y_{t,2}, y_{t,1}) \text{ and } x_{t,agent} > x_{t,i}, \\ 0, & \text{otherwise.} \end{cases} \quad (21)$$

Table 2: Parameters for the environment Simple-OA

Parameter	Description	Value
N_{obstacle}	number of obstacles	2
x_{scale}	scaling factor for observation	1500 m
y_{scale}	scaling factor for observation	1700 m
y_{max}	end zone for obstacles	200 m
Δy	distance between obstacles	50 m

3.4 Environment Complex-OA

The environment Complex-OA represents a more realistic environment for obstacle avoidance. In contrast to the environment Simple-OA, where the agent had to anticipate a single obstacle trajectory, the agent now has to anticipate several trajectories simultaneously. A further challenge is to prioritize those trajectories regarding their potential of leading to a collision in the near future.

We define our observation space with $N_{\text{obstacle}} = 12$. Further, we define the set of obstacles that should only be passed, from the perspective of the agent, on the right side in lateral direction as $\mathcal{M}_{\text{right}} = \{1, \dots, N_{\text{obstacle}}/2\}$. Consequently, the remaining obstacles should be passed left and are denoted $\mathcal{M}_{\text{left}} = \{N_{\text{obstacle}}/2 + 1, \dots, N_{\text{obstacle}}\}$. Similar to the Simple-OA, we initialize the agent’s dynamics to zero, except the longitudinal speed $\dot{x}_{0,\text{agent}}$, that is sampled uniformly at random from the interval $[1 \text{ m/s}, v_{x,\text{max}}]$. We define $TTC_{t,i}$ as the agent’s time-to-collision with an obstacle $i \in \mathcal{M}$ in longitudinal direction at time step t . Negative values for $TTC_{t,i}$ relate to obstacles that already passed the agent in the longitudinal direction. If for two obstacles $k, l \in \mathcal{M}_{\text{right}}$ holds: $TTC_{t,k} < 0$, $TTC_{t,l} < 0$, and $TTC_{t,k} < TTC_{t,l}$, we replace obstacle k as shown in Figure 5. Its new time-to-collision is randomly sampled from:

$$TTC_{t,k} \sim \mathcal{U} \left(\left[\max_{j \in \mathcal{M}_{\text{right}}} (TTC_{t,j}), \max_{j \in \mathcal{M}_{\text{right}}} (TTC_{t,j}) + \Delta TTC_{\text{max}} \right] \right), \quad (22)$$

where ΔTTC_{max} is the maximal temporal distance for the new placement of an obstacle. This parameter affects the number of obstacles being passed in a certain time interval and is therefore a crucial design element of this environment. The same replacement procedure is applied for obstacles with passing rule ‘left’.

Having computed the new value for $TTC_{t,i}$ for a replaced obstacle $i \in \mathcal{M}$ at time step t , the new dynamics of the obstacle need to be set. First, we draw values for $\dot{x}_{t,i}$ and $\dot{y}_{t,i}$ from uniform distributions:

$$\dot{x}_{t,i} \sim \mathcal{U}([-v_{x,\text{max}}, v_{x,\text{max}}]), \quad (23)$$

$$\dot{y}_{t,i} \sim \mathcal{U}([-v_{y,\text{max}}, v_{y,\text{max}}]). \quad (24)$$

Second, the new longitudinal position can be set according to:

$$x_{t,i} = (\dot{x}_{t,\text{agent}} - \dot{x}_{t,i})TTC_{t,i} + x_{t,\text{agent}}. \quad (25)$$

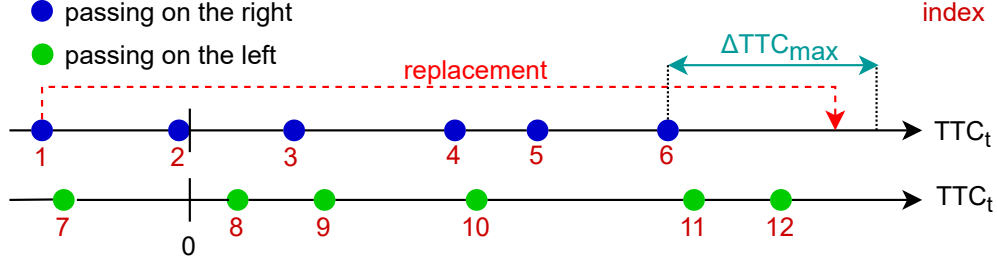


Figure 5: Replacement of an obstacle (obstacle 1) since two obstacles with the same passing rule already passed the agent (negative time-to-collision). The obstacle’s new $TTC_{t,1}$ is set uniformly at random in the time interval colored turquoise with the length of ΔTTC_{\max} .

Third, having the lateral speed of the replaced obstacle set, we generate the new lateral position with the help of a predefined, stochastic trajectory $y_{t,\text{traj}}$. This lateral trajectory is computed at the beginning of an episode and is based on a smoothed AR(1) process (Tsay, 2010), whose parameters reflect the kinematics of the agent. Figure 6 shows a replacement situation identical to Figure 5 and illustrates how this trajectory is used to define the new lateral position for a replaced obstacle. One can think of this stochastic process as an approximate trajectory the agent has to follow to avoid collisions with obstacles. In the following, we define the smoothed AR(1) process and give a detailed explanation about the replacement of an obstacle based on that process.

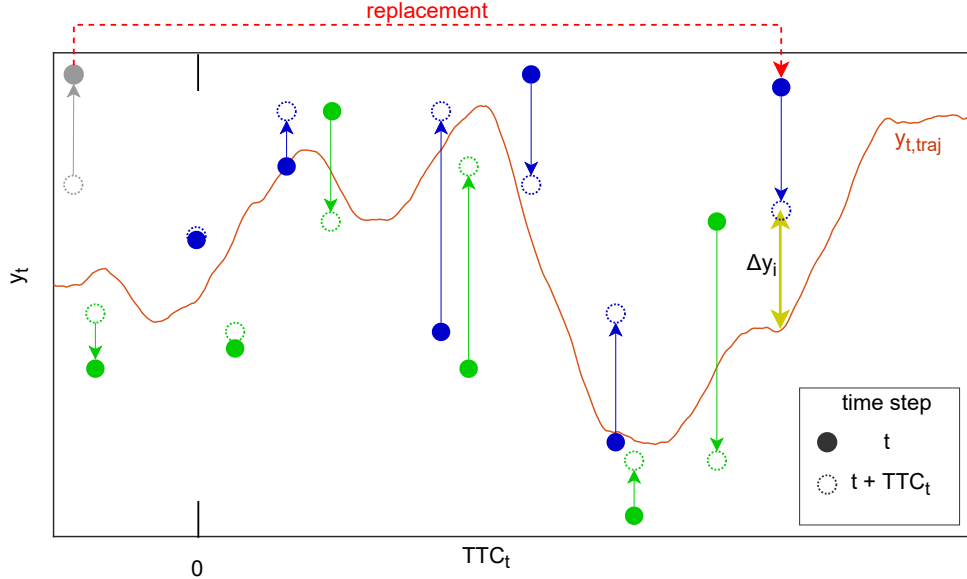


Figure 6: Replacement of an obstacle identical to the situation in Figure 5 but with additional information about lateral positions of obstacles.

The AR(1) process is defined as:

$$X_{t+1} = \phi X_t + u, \quad \text{where } u \sim \mathcal{N}(0, \sigma_{\text{AR}}^2), \quad (26)$$

with auto-regressive parameter ϕ and variance σ_{AR} . The parameters have been designed to model a lateral trajectory the agent can approximately follow under acceleration and velocity constraints represented by $a_{y,max}$ and $v_{y,max}$. To reduce the noise, we exponentially smooth the AR(1) process:

$$y_{t,traj} = \begin{cases} X_0, & \text{for } t = 0, \\ \beta X_t + (1 - \beta)y_{t-1,traj}, & t > 0, \end{cases} \quad (27)$$

where β defines the smoothing factor. Based on this trajectory and having already computed $TTC_{t,i}$, $x_{t,i}$, $\dot{x}_{t,i}$, and $\dot{y}_{t,i}$ via (22), (23), (24), and (25), one more step is needed to set the new lateral position $y_{t,i}$ for a replaced obstacle $i \in \mathcal{M}$ at time step t .

We define Δy_i as the absolute difference between an obstacle's lateral position $y_{t,i}$ and the defined trajectory $y_{t,traj}$ when agent and obstacle are at the same longitudinal position ($TTC_{t,i} = 0$):

$$\Delta y_i = |y_{t,i} - y_{t,traj}| \quad \text{for } TTC_{t,i} = 0, \quad (28)$$

shown yellow in Figure 6. To force our agent to move approximately along the trajectory $y_{t,traj}$, the positional difference Δy_i should be small, thus being another crucial design parameter to adjust the complexity of the environment. Every time an obstacle i is replaced, the variable Δy_i is sampled from a normal distribution:

$$\Delta y_i \sim \mathcal{N}(\mu_{\Delta y}, \sigma_{\Delta y}^2), \quad (29)$$

and lower-bounded to Δy_{min} :

$$\Delta y_i = \max(\Delta y_{min}, \Delta y_i). \quad (30)$$

By changing the parameters Δy_{min} , $\sigma_{\Delta y}^2$, and Δy_{min} , one can adjust how close the obstacles are coming to the trajectory $y_{t,traj}$ when obstacle and agent are at the same longitudinal position. The chosen values for those parameters can be found in Table 3. Finally, the lateral position for obstacles $i_R \in \mathcal{M}_{right}$ is computed via:

$$y_{t,i_R} = y_{t,traj} + \Delta y_{i_R} - \dot{y}_{t,i_R} TTC_{t,i_R}, \quad (31)$$

and for obstacles $i_L \in \mathcal{M}_{left}$ via:

$$y_{t,i_L} = y_{t,traj} - \Delta y_{i_L} - \dot{y}_{t,i_L} TTC_{t,i_L}. \quad (32)$$

Figure 6 shows the final lateral position and time-to-collision for a replaced obstacle as a filled circle.

In the following, we detail the reward function used to train the RL agent. The aim of this function is to penalize collisions with obstacles, to consider the passing rule for each obstacle, and to penalize getting in the proximity of an obstacle. Considering all these factors, we define the reward for an obstacle $i_R \in \mathcal{M}_{right}$ at time step t as:

$$r_{t,i_R} = -\frac{\varphi(TTC_{t,i_R}/\sigma_{TTC})}{\varphi(0)} \frac{\varphi\{\max(0, y_{t,i_R} - y_{t,agent})/\sigma_y\}}{\varphi(0)}, \quad (33)$$

and for an obstacle $i_L \in \mathcal{M}_{left}$:

$$r_{t,i_L} = -\frac{\varphi(TTC_{t,i_L}/\sigma_{TTC})}{\varphi(0)} \frac{\varphi\{\max(0, y_{t,agent} - y_{t,i_L})/\sigma_y\}}{\varphi(0)}, \quad (34)$$

where $\varphi(x)$ denotes the density function of the standard normal distribution and the parameters σ_{TTC}^2 and σ_y^2 describe variances. Since we are only interested in penalizing the agent with respect to the closest obstacle, the reward at time step t is defined to be the minimum of all obstacle rewards:

$$r_t = \min_{i \in \mathcal{M}}(r_{t,i}). \quad (35)$$

Figure 7 illustrates the reward function for twelve obstacles. As one can see, violating the passing rule is penalized in the same magnitude as colliding with an obstacle. Furthermore, the agent is also penalized when getting close to an obstacle, adjusted by the parameters σ_{TTC}^2 and σ_y^2 . At this point it is important to mention that when the agent passes obstacles with different relative longitudinal speeds, the agent should be rewarded in the same way. Therefore, we use the time-to-collision instead of the position in longitudinal direction to model the reward function.

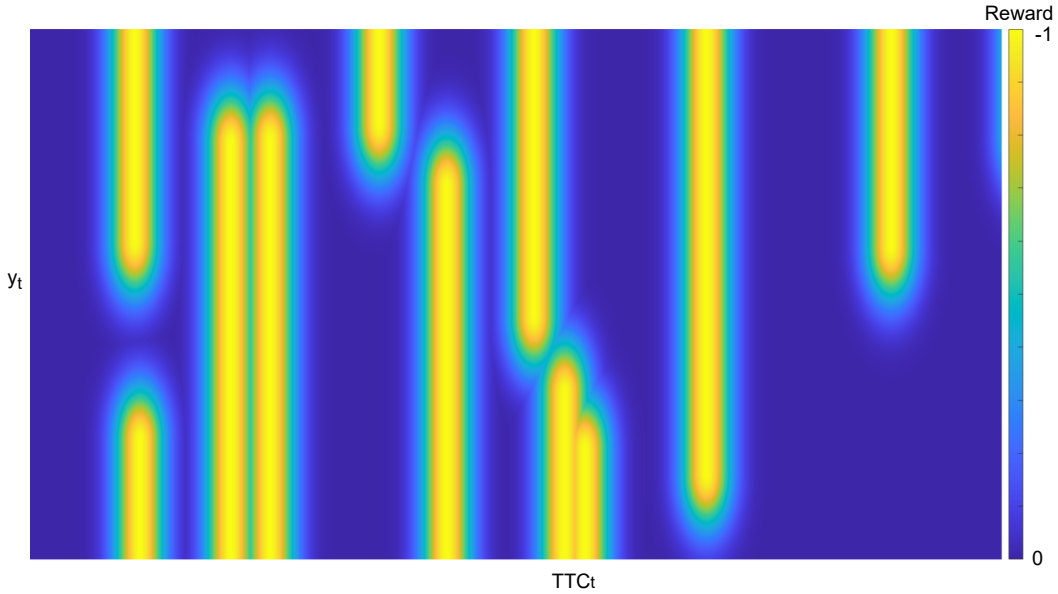


Figure 7: Reward function for the environment Complex-OA.

Table 3 contains a description and the chosen values for all Complex-OA parameters.

Table 3: Parameters for the environment Complex-OA

Parameter	Description	Value
N_{obstacle}	number of obstacles	12
x_{scale}	scaling factor for observation	3000 m
y_{scale}	scaling factor for observation	3000 m
ΔTTC_{max}	maximal temporal distance for replacing an obstacle	300 s
ϕ	AR(1) process parameter	0.99
σ_{AR}	normal distribution variance	28.3 m ²
β	smoothing factor	0.03
$\mu_{\Delta y}$	normal distribution mean	100 m
$\sigma_{\Delta y}^2$	normal distribution variance	50 m ²
Δy_{min}	minimum bound for Δy	40 m
σ_y^2	normal distribution variance	25 m ²
σ_{TTC}^2	normal distribution variance	25 s ²

4 Results

We train the TD3, LSTM-TD3, and TD3-FS algorithms for both environments, Simple-OA and Complex-OA. The frame-stacking consists of expanding the current observation with the observations from the last two steps to match the LSTM-TD3 information set with $l = 2$. The training setup and hyperparametrization is identical to Section 2.4, except that we train for $15 \cdot 10^6$ time steps since we could not observe convergence beforehand. Regarding the Simple-OA, the return yields a straightforward interpretation since, e.g., a return of 80 implies that 9 out of the 10 evaluation episodes have been successful. In the following, we summarize the main findings of this investigation:

1. For both environments, the algorithms perform worse if there is no velocity information.
2. In the environment Simple-OA, the TD3 fails nearly completely if no velocity information is available since the agent rarely passes between the obstacles. In the contrary, LSTM-TD3 and TD3-FS are significantly better than TD3 and perform on a comparable level, although still not reaching the MDP performance.
3. In the environment Simple-OA, the LSTM-TD3 algorithm learns a near optimal policy in a fraction of the considered training steps and overall dramatically stabilizes the learning process compared to the TD3 and TD3-FS approaches for the MDP scenario.
4. In the environment Complex-OA, all algorithms perform similarly in both observation space configurations. However, the TD3-FS appears slightly worse than its two competitors.

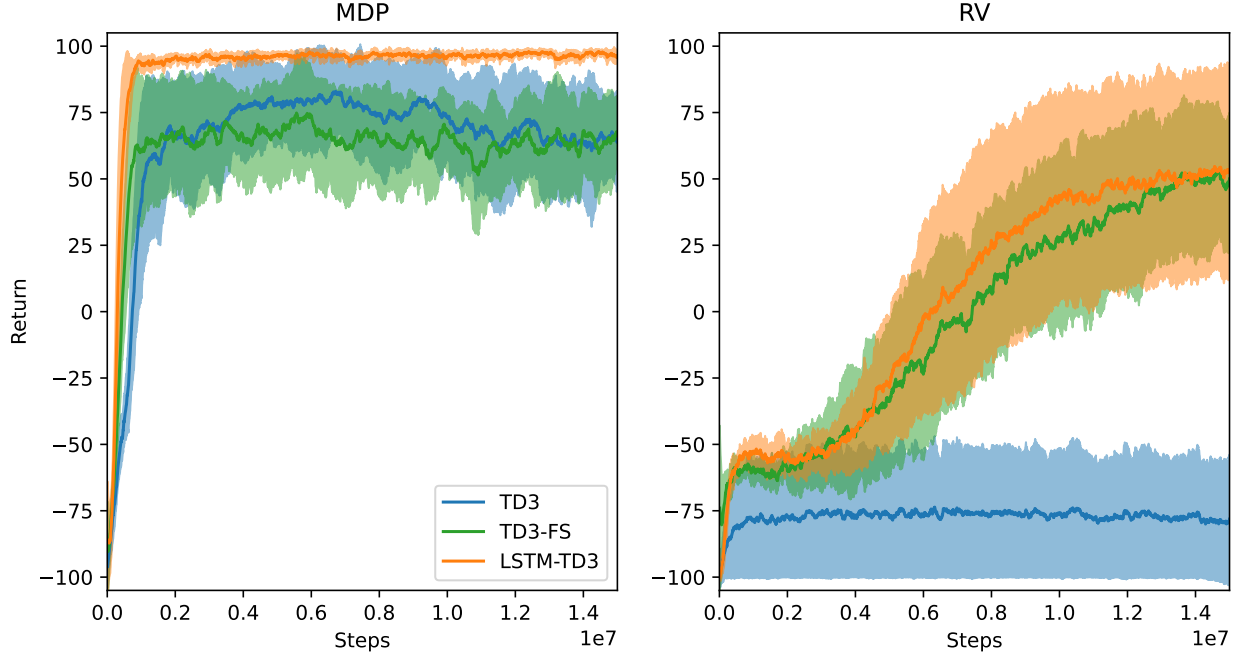


Figure 8: Performance comparison of the considered agents in the environment Simple-OA. Results are averaged over 10 independent runs. The shaded area are two standard deviations over the runs.

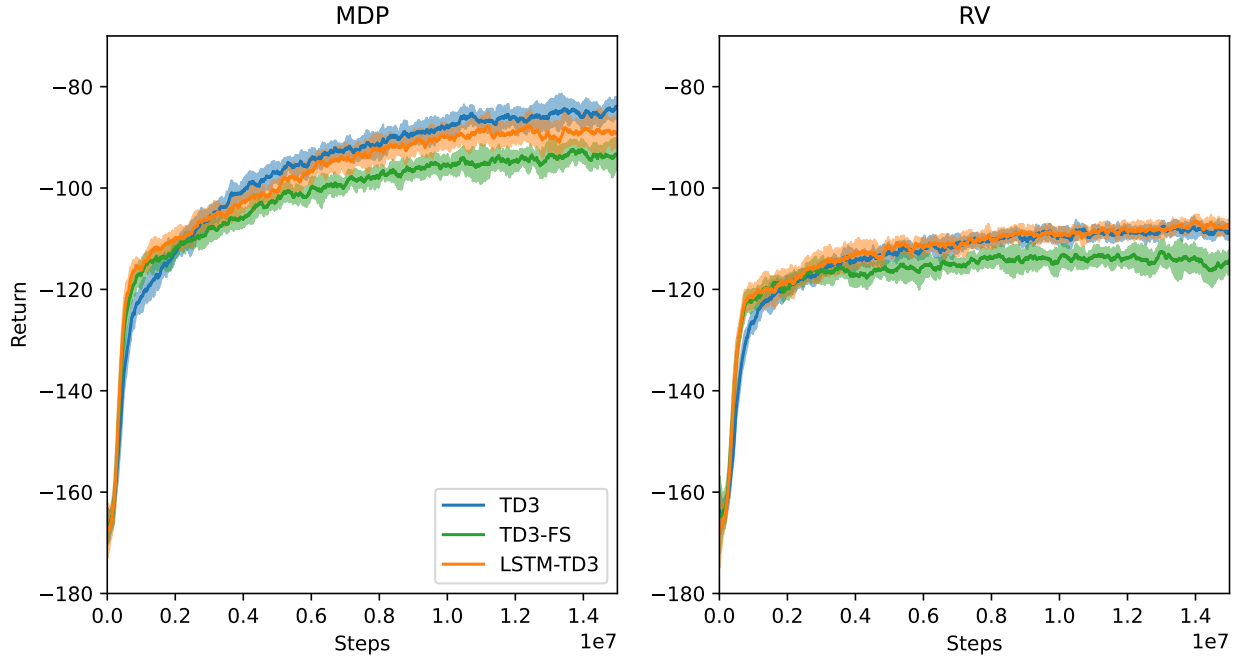


Figure 9: Performance comparison of the considered agents in the environment Complex-OA. Results are averaged over 10 independent runs. The shaded area are two standard deviations over the runs.

5 Discussion

In the environment Simple-OA, the optimal policy simply requires anticipating one particular trajectory of a randomly generated obstacle pair, representing a basic analytical task. Astonishingly, even with all necessary information, both agents without recurrency in their respective function approximators cannot master this task entirely. Similarly surprising, although the recurrent and frame-stacking approaches perform significantly better than a 'plain' agent in the RV scenario, they are even in this simple task not able to achieve a similar return level as in the MDP case.

In contrast to the environment Simple-OA, the Complex-OA scenario yields two additional difficulties. First, several trajectories need to be simultaneously anticipated. Second, this information needs to be processed by prioritizing the trajectories regarding their potential of generating a collision in the near future. All agents perform reliably better when provided with the complete state information for this environment while displaying a performance drop in the RV scenario. This is in line with the findings from the Simple-OA. Remarkably, in contrast to the first task, the recurrency and frame-stacking approaches do not help to solve the Complex-OA. More precisely, the recurrent agent learns a performance-wise equal policy like the 'plain' agent. This leads to the assumption that the recurrent agent also solely relies on positional information without developing the ability to anticipate and prioritize the obstacles' trajectories correctly. We argue that this can be explained by the increased complexity of the environmental dynamics contrary to the Simple-OA scenario, which is an isolated investigation concerning only one relevant trajectory. To guarantee the robustness of these findings against different specifications of the environments, we tested for a variety of different settings by changing: the number of obstacles, the maximum temporal distance for replacing an obstacle, the smoothed AR(1) process parametrization, the obstacle distance to the AR(1)-based trajectory when longitudinal TTC is zero, the maximum acceleration and velocities for agent and obstacles, the reward configuration, and the RL algorithm hyperparameters. Throughout all these specifications, the main findings are qualitatively unchanged.

Regarding our initial Hypothesis 1 & 2, we can reject both of them. The recurrent layers as well as frame-stacking approaches are not able to consistently replace missing velocity information in the observation space. However, in simplified scenarios, they are able to significantly boost performance and stabilize the overall training procedure.

6 Conclusion

Dynamic obstacle avoidance is a fundamental task in many real-world application domains, e.g., self-driving cars, service robots, or unmanned surface vehicles. A core element of successfully mastering obstacle avoidance tasks is the precise anticipation of trajectories of relevant obstacles. However, real-world systems rely on sensor data that is often limited to positional information about moving obstacles or vehicles without explicitly providing velocity-related information. From a physical perspective, trajectories cannot be predicted solely from current positional information, and approaches like recurrency or frame-stacking are expected to yield improved performance. We analyze the severity of missing velocity

information and evaluate the potential of recurrency and frame-stacking approaches. Therefore, we define a traffic type independent environment with variants of different complexity, in which we test several model-free RL agents. Across all agents, we found that the lack of velocity information significantly harms the performance. The approaches of recurrency and frame-stacking cannot reliably replace missing velocity information in the observation space. In complex dynamic obstacle avoidance scenarios, which require anticipating and prioritizing the trajectories of several objects, all agents struggle to reach the performance they achieve with complete information. However, in simplified scenarios, where the anticipation of a single trajectory is required, recurrency and frame-stacking can significantly improve the agent’s ability to learn an appropriate obstacle avoidance behavior even when only positional information is available. Although it does not always improve the agent’s performance, we generally recommend to integrate recurrency in the function approximators when only positional sensor data is available.

Acknowledgements

This work was partially funded by BAW - Bundesanstalt für Wasserbau (Mikrosimulation des Schiffsverkehrs auf dem Niederrhein).

References

- Abadi, M., Barham, P., Chen, J., Chen, Z., Davis, A., Dean, J., Devin, M., Ghemawat, S., Irving, G., Isard, M., Kudlur, M., Levenberg, J., Monga, R., Moore, S., Murray, D. G., Steiner, B., Tucker, P., Vasudevan, V., Warden, P., Wicke, M., Yu, Y., and Zheng, X. TensorFlow: A system for large-scale machine learning. *12th USENIX Symposium on Operating Systems Design and Implementation (OSDI 16)*, 2016, 265–283.
- Althé, F. and de La Fortelle, A. An LSTM network for highway trajectory prediction. *IEEE 20th International Conference on Intelligent Transportation Systems (ITSC)*, 2017, 353–359.
- Bellman, R. The theory of dynamic programming. *Bulletin of the American Mathematical Society*, 1954, **60**, 503–515.
- Bhopale, P., Kazi, F., and Singh, N. Reinforcement Learning Based Obstacle Avoidance for Autonomous Underwater Vehicle. *Journal of Marine Science and Application*, 2019, **18**.
- Canny, J. and Reif, J. 1987, New Lower Bound Techniques for Robot Motion Planning Problems. in *Proceedings of the 28th Annual Symposium on Foundations of Computer Science*, USA: IEEE Computer Society, SFCS ’87, p. 49–60.
- Chen, C., Chen, X.-Q., Ma, F., Zeng, X.-J., and Wang, J. A knowledge-free path planning approach for smart ships based on reinforcement learning. *Ocean Engineering*, 2019, **189**, 106299.
- Cimurs, R., Lee, J. H., and Suh, I. H. Goal-Oriented Obstacle Avoidance with Deep Reinforcement Learning in Continuous Action Space. *Electronics*, 2020, **9**, 411.

- Duguleana, M. and Mogan, G. Neural networks based reinforcement learning for mobile robots obstacle avoidance. *Expert Systems with Applications*, 2016, **62**, 104–115.
- Ellenberger, B. 2021, pybullet-gym. <https://github.com/benelot/pybullet-gym>.
- Fiorini, P. and Shiller, Z. Motion Planning in Dynamic Environments Using Velocity Obstacles. *The International Journal of Robotics Research*, 1998, **17**, 760–.
- Fujimoto, S., Hoof, H., and Meger, D. Addressing function approximation error in actor-critic methods. *International Conference on Machine Learning*, 2018, 1587–1596.
- Goerzen, C., Kong, Z., and Mettler, B. A Survey of Motion Planning Algorithms from the Perspective of Autonomous UAV Guidance. *Journal of Intelligent and Robotic Systems*, 2010, **57**, 65–100.
- Goodfellow, I., Bengio, Y., and Courville, A., *Deep Learning*, 2016, MIT press.
- Heess, N., Hunt, J. J., Lillicrap, T. P., and Silver, D. Memory-based control with recurrent neural networks. *arXiv preprint arXiv:1512.04455*, 2015.
- Hochreiter, S. and Schmidhuber, J. Long short-term memory. *Neural computation*, 1997, **9**, 1735–1780.
- Jenie, Y., Van Kampen, E.-J., De Visser, C., Ellerbroek, J., and Hoekstra, J. Three-Dimensional Velocity Obstacle Method for Uncoordinated Avoidance Maneuvers of Unmanned Aerial Vehicles. *Journal of Guidance, Control, and Dynamics*, 2016, **39**, 1–12.
- Kaelbling, L. P., Littman, M. L., and Cassandra, A. R. Planning and acting in partially observable stochastic domains. *Artificial intelligence*, 1998, **101**, 99–134.
- Kingma, D. P. and Ba, J. Adam: A method for stochastic optimization. *arXiv preprint arXiv:1412.6980*, 2014.
- Kuwata, Y., Wolf, M. T., Zarzhitsky, D., and Huntsberger, T. L. Safe Maritime Autonomous Navigation With COLREGS, Using Velocity Obstacles. *IEEE Journal of Oceanic Engineering*, 2014, **39**, 110–119.
- Lillicrap, T. P., Hunt, J. J., Pritzel, A., Heess, N., Erez, T., Tassa, Y., Silver, D., and Wierstra, D. Continuous control with deep reinforcement learning. *arXiv preprint arXiv:1509.02971*, 2015.
- Meng, L., Gorbet, R., and Kulić, D. Memory-based Deep Reinforcement Learning for POMDP. *arXiv preprint arXiv:2102.12344*, 2021.
- Mnih, V., Kavukcuoglu, K., Silver, D., Rusu, A. A., Veness, J., Bellemare, M. G., Graves, A., Riedmiller, M., Fidjeland, A. K., Ostrovski, G., et al. Human-level control through deep reinforcement learning. *Nature*, 2015, **518**, 529–533.
- Ni, T., Eysenbach, B., and Salakhutdinov, R. Recurrent Model-Free RL is a Strong Baseline for Many POMDPs. *arXiv preprint arXiv:2110.05038*, 2021.

- Paszke, A., Gross, S., Massa, F., Lerer, A., Bradbury, J., Chanan, G., Killeen, T., Lin, Z., Gimelshein, N., Antiga, L., Desmaison, A., Köpf, A., Yang, E., DeVito, Z., Raison, M., Tejani, A., Chilamkurthy, S., Steiner, B., Fang, L., Bai, J., and Chintala, S. Pytorch: An imperative style, high-performance deep learning library. *Advances in neural information processing systems*, 2019, **32**, 8026–8037.
- Roghair, J., Ko, K., Asli, A. E. N., and Jannesari, A. A Vision Based Deep Reinforcement Learning Algorithm for UAV Obstacle Avoidance. *CoRR*, 2021, **abs/2103.06403**.
- Schaul, T., Quan, J., Antonoglou, I., and Silver, D. Prioritized experience replay. *Proceedings of the IEEE International Conference on Learning Representations*, 2016.
- Silver, D., Lever, G., Heess, N., Degris, T., Wierstra, D., and Riedmiller, M. Deterministic policy gradient algorithms. *International Conference on Machine Learning*, 2014, 387–395.
- Silver, D., Schrittwieser, J., Simonyan, K., Antonoglou, I., Huang, A., Guez, A., Hubert, T., Baker, L., Lai, M., Bolton, A., Chen, Y., Lillicrap, T., Hui, F., Sifre, L., Driessche, G., Graepel, T., and Hassabis, D. Mastering the game of Go without human knowledge. *Nature*, 2017, **550**, 354–359.
- Sutton, R. S. and Barto, A. G., *Reinforcement Learning: An Introduction*, 2018, MIT press.
- Treiber, M. and Kesting, A. 2013, *Elementary Car-Following Models*, Berlin, Heidelberg: Springer Berlin Heidelberg, pp. 157–180.
- Triebel, R., Arras, K., Alami, R., Beyer, L., Breuers, S., Chatila, R., Chetouani, M., Cremers, D., Evers, V., Fiore, M., Hung, H., Ramírez, O. A. I., Joosse, M., Khambhaita, H., Kucner, T., Leibe, B., Lilienthal, A. J., Linder, T., Lohse, M., Magnusson, M., Okal, B., Palmieri, L., Rafi, U., van Rooij, M., and Zhang, L. 2016, *SPENCER: A Socially Aware Service Robot for Passenger Guidance and Help in Busy Airports*, Cham: Springer International Publishing, pp. 607–622.
- Tsay, R. S., *Analysis of Financial Time Series*, 2010, New Jersey: John Wiley & Sons.
- Urmson, C., Anhalt, J., Bagnell, D., Baker, C., Bittner, R., Clark, M., Dolan, J., Duggins, D., Galatali, T., Geyer, C., Gittleman, M., Harbaugh, S., Hebert, M., Howard, T., Kolski, S., Kelly, A., Likhachev, M., Mcnaughton, M., Miller, N., and Ferguson, D. Autonomous Driving in Urban Environments: Boss and the Urban Challenge. *Journal of Field Robotics*, 2008, **25**, 425–466.
- Wang, C., Wang, J., Shen, Y., and Zhang, X. Autonomous Navigation of UAVs in Large-Scale Complex Environments: A Deep Reinforcement Learning Approach. *IEEE Transactions on Vehicular Technology*, 2019, **PP**, 1–1.
- Wang, Y., He, H., and Sun, C. Learning to Navigate Through Complex Dynamic Environment With Modular Deep Reinforcement Learning. *IEEE Transactions on Games*, 2018, **10**, 400–412.
- Watkins, C. J. and Dayan, P. Q-learning. *Machine learning*, 1992, **8**, 279–292.

- Wilkie, D., van den Berg, J. P., and Manocha, D. Generalized velocity obstacles. *2009 IEEE/RSJ International Conference on Intelligent Robots and Systems*, 2009, 5573–5578.
- Xie, L., Wang, S., Markham, A., and Trigoni, N. 2017, Towards Monocular Vision based Obstacle Avoidance through Deep Reinforcement Learning. .
- Xu, W., Liu, X., and Chu, X. Simulation models of vessel traffic flow in inland multi-bridge waterway. *2015 International Conference on Transportation Information and Safety (ICTIS)*, 2015, 505–511.
- Xu, X., Lu, Y., Liu, X., and Zhang, W. Intelligent collision avoidance algorithms for USVs via deep reinforcement learning under COLREGs. *Ocean Engineering*, 2020, **217**, 107704.
- Yan, L., Chang, X., Wang, N., Tian, R., Zhang, L., and Liu, W. Learning how to avoid obstacles: A numerical investigation for maneuvering of self-propelled fish based on deep reinforcement learning. *International Journal for Numerical Methods in Fluids*, 2021, **93**.

A Algorithm details and hyperparameter

Algorithm 2: TD3 algorithm following [Fujimoto et al. \(2018\)](#).

Randomly initialize critics $Q^{\omega_1}, Q^{\omega_2}$ and actor μ^θ
Initialize target critics $Q^{\omega'_1}, Q^{\omega'_2}$ and target actor $\mu^{\theta'}$ with $\omega'_1 \leftarrow \omega_1, \omega'_2 \leftarrow \omega_2, \theta' \leftarrow \theta$
Initialize replay buffer \mathcal{D}
Receive initial state s_1 from environment
for $t = 1, T$ **do**
 Acting
 Select action with exploration noise: $a_t = \mu^\theta(s_t) + \epsilon, \quad \epsilon \sim \mathcal{N}(0, \sigma)$
 Execute a_t , receive reward r_{t+1} , new state s_{t+1} , and done flag d_t
 Store transition $(s_t, a_t, r_{t+1}, s_{t+1}, d_t)$ to \mathcal{D}
 Learning
 Sample random mini-batch of transitions $(s_i, a_i, r_{i+1}, s_{i+1}, d_i)_{i=1}^N$ from \mathcal{D}
 Calculate targets:

$$\tilde{a}_{i+1} = \mu^{\theta'}(s_{i+1}) + \tilde{\epsilon}, \quad \tilde{\epsilon} \sim \text{clip}\{\mathcal{N}(0, \tilde{\sigma}), -c, c\},$$

$$y_i = r_{i+1} + \gamma(1 - d_i) \min_{j=1,2} Q^{\omega'_j}(s_{i+1}, \tilde{a}_{i+1}).$$
 Update critics: $\omega_j \leftarrow \min_{\omega_j} N^{-1} \sum_i \{y_i - Q^{\omega_j}(s_i, a_i)\}^2$
 if $t \bmod d$ **then**
 | Update actor: $\theta \leftarrow \max_{\theta} N^{-1} \sum_i Q^{\omega_1} \{s_i, \mu^\theta(s_i)\}$
 | Update target networks via (4)
 end
 End of episode handling
 if d_t **then**
 | Reset environment to an initial state s_{t+1}
 end
end

Hyperparameter	Value
Discount factor γ	0.99
Batch size N	32
Replay buffer size $ \mathcal{D} $	10^5
Learning rate actor α_{actor}	10^{-4}
Learning rate critic α_{critic}	10^{-4}
Target update rate τ	0.001
Random start step N_{start_step}	5 000
Update start step N_{update_after}	5 000
Optimizer	Adam
Exploration noise σ	0.1
Target policy smoothing $\tilde{\sigma}$	0.2
Target policy smoothing c	0.5
Policy update delay d	2
History length l	2

Table 4: List of hyperparameters used in both TD3 and LSTM-TD3. N_{start_step} means that at the beginning of each training process, the agent performs N_{start_step} steps completely at random for initial exploration. N_{update_after} is the step after which critic and actor updates are performed.